Understanding the contribution of mode area and slow light to the effective Kerr nonlinearity of waveguides

Shahraam Afshar V.,[1*] **T. M. Monro,**[1] **and C. Martijn de Sterke**[2]

[1] *Institute for Photonics and Advanced Sensing (IPAS), The University of Adelaide, 5005, Australia*

[2] *Centre for Ultrahigh Bandwidth Devices for Optical Systems (CUDOS) and Institute of Photonics and Optical Science (IPOS), School of Physics, The University of Sydney, NSW 2006, Australia*

**shahraam.afshar@adelaide.edu.au*

Abstract: We resolve the ambiguity in existing definitions of the effective area of a waveguide mode that have been reported in the literature by examining which definition leads to an accurate evaluation of the effective Kerr nonlinearity. We show that the effective nonlinear coefficient of a waveguide mode can be written as the product of a suitable average of the nonlinear coefficients of the waveguide's constituent materials, the mode's group velocity and a new suitably defined effective mode area. None of these parameters on their own completely describe the strength of the nonlinear effects of a waveguide.

OCIS codes: (190.4370) Nonlinear optics, fibers; (190.3270) Kerr effect; (190.4360) Nonlinear optics, devices; (130.4310) Integrated optics (Nonlinear); (060.4005) Microstructured fibers; (060.5530) Pulse propagation and temporal solitons.

References and links

1. P. N. Butcher and D. Cotter, *The Elements of Nonlinear Optics* (Cambridge University, 1990).
2. P. Agrawal, *Nonlinear Fiber Optics* (Academic press, 2007).
3. I. D. Rukhlenko, M. Premaratne, S. Member, and G. P. Agrawal, "Nonlinear silicon photonics : Analytical tools," IEEE J. Selec. Quantum Electron. **16**, 200–215 (2010).
4. I. D. Rukhlenko, M. Premaratne, and G. P. Agrawal, "Effective mode area and its optimization in silicon-nanocrystal waveguides," Opt. Lett. **37**, 2295–2297 (2012).
5. M. Soljačić, S. G. Johnson, S. Fan, M. Ibanescu, E. Ippen, and J. D. Joannopoulos, "Photonic-crystal slow-light enhancement of nonlinear phase sensitivity," J. Opt. Soc. Am. B **19**, 2052–2059 (2002).
6. T. Baba, "Slow light in photonic crystals," Nature Photonics **2**, 465–473 (2008).
7. B. Corcoran, C. Monat, C. Grillet, D. J. Moss, B. J. Eggleton, T. P. White, L. O'Faolain, and T. F. Krauss, "Green light emission in silicon through slow-light enhanced third-harmonic generation in photonic-crystal waveguides," Nature Photonics **3**, 206 – 210 (2009).
8. N.-C. Panoiu, J. McMillan, and C. W. Wong, "Theoretical analysis of pulse dynamics in silicon photonic crystal wire waveguides," IEEE J. Selec. Quantum Electron. **16**, 257–266 (2010).
9. V. R. Almeida, Q. Xu, C. A. Barrios, and M. Lipson, "Guiding and confining light in void nanostructure," Opt. Lett. **29**, 1209–1211 (2004).
10. O. Boyraz, P. Koonath, V. Raghunathan, and B. Jalali, "All optical switching and continuum generation in silicon waveguides," Opt. Express **12**, 4094–4102 (2004).
11. C. Koos, P. Vorreau, T. Vallaitis, P. Dumon, W. Bogaerts, R. Baets, B. Esembeson, I. Biaggio, T. Michinobu, F. Diederich, W. Freude, and J. Leuthold, "All-optical high-speed signal processing with silicon-organic hybrid slot waveguides," Nature Photonics **3**, 216–219 (2009).
12. W. Astar, J. B. Driscoll, X. Liu, J. I. Dadap, W. M. J. Green, Y. A. Vlasov, G. M. Carter, and R. M. Osgood. Jr., "Tunable wavelength conversion by xpm in a silicon nanowire, and the potential for xpm-multicasting," J. Lightwave Technol. **28**, 2499–2511 (2010).

#191963 - $15.00 USD Received 10 Jun 2013; revised 12 Jul 2013; accepted 14 Jul 2013; published 26 Jul 2013

13. R. K. W. Lau, M. Ménard, Y. Okawachi, M. A. Foster, A. C. Turner-Foster, R. Salem, M. Lipson, and A. L. Gaeta, "Continuous-wave mid-infrared frequency conversion in silicon nanowaveguides," Opt. Lett. **36**, 1263–1265 (2011).
14. J. Leuthold, C. Koos, and W. Freude, "Nonlinear silicon photonics," Nature Photonics **4**, 535–544 (2010).
15. M. Pelusi, F. Luan, T. D. Vo, M. R. E. Lamont, S. J. Madden, D. A. Bulla, D.-Y. Choi, B. Luther-Davis, and B. J. Eggleton, "Photonic-chip-based radio-frequency spectrum analyser with terahertz bandwidth," Nature Photonics **3**, 139–143 (2009).
16. X. Gai, T. Han, A. Prasad, S. Madden, D.-Y. Choi, R. Wang, D. Bulla, and B. Luther-Davies, "Progress in optical waveguides fabricated from chalcogenide glasses," Opt. Express **18**, 26635–26646 (2010).
17. B. J. Eggleton, B. Luther-Davies, and K. Richardson, "Chalcogenide photonics," Nature Photonics **5**, 141–148 (2011).
18. P. Petropoulos, T. M. Monro, W. Belardi, K. Furusawa, J. H. Lee, and D. J. Richardson, "2R-regenerative all-optical switch based on a highly nonlinear holey fiber," Opt. Lett. **26**, 1233–1235 (2001).
19. H. Ebendorff-Heidepriem, P. Petropoulos, S. Asimakis, V. Finazzi, R. C. Moore, K. Frampton, F. Koizumi, D. J. Richardson, and T. M. Monro, "Bismuth glass holey fibers with high nonlinearity," Opt. Express **12**, 5082 (2004).
20. S. Afshar V., W. Q. Zhang, H. Ebendorff-Heidepriem, and T. M. Monro, "Small core optical waveguides are more nonlinear than expected: experimental confirmation," Opt. Lett. **34**, 3577–3579 (2009).
21. G. Qin, X. Yan, C. Kito, M. Liao, T. Suzuki, A. Mori, and Y. Ohishi, "Highly nonlinear tellurite microstructured fibers for broadband wavelength conversion and flattened supercontinuum generation," J. Appl. Phys. **107**, 043108 (2010).
22. F. Poletti, X. Feng, G. M. Ponzo, M. N. Petrovich, W. H. Loh, and D. J. Richardson, "All-solid highly nonlinear singlemode fibers with a tailored dispersion profile," Opt. Express **19**, 66–80 (2011).
23. S. Maier, "Plasmonics: Metal nanostructures for subwavelength photonic devices," IEEE J. Selec. Quantum Electron. **12**, 1214–1220 (2006).
24. D. K. Gramotnev and S. I. Bozhevolnyi, "Plasmonics beyond the diffraction limit," Nature Photonics **4**, 83–91 (2010).
25. M. Foster, K. Moll, and A. Gaeta, "Optimal waveguide dimensions for nonlinear interactions." Opt. Express **12**, 2880–7 (2004).
26. P. Sanchis, J. Blasco, S. Member, A. Martínez, and J. Martí, "Design of silicon-based slot waveguide configurations for optimum nonlinear performance," J. Lightwave Technol. **25**, 1298–1305 (2007).
27. S. Afshar V. and T. M. Monro, "A full vectorial model for pulse propagation in emerging waveguides with subwavelength structures part i: Kerr nonlinearity," Opt. Express **17**, 2298–2318 (2009).
28. J. Lægsgaard, "Modeling of nonlinear propagation in fiber tapers," J. Opt. Soc. Am. B **29**, 3183–3191 (2012).
29. X. Chen, N. C. Panoiu, and R. M. Osgood, "Theory of raman-mediated pulsed amplification in silicon-wire waveguides," IEEE J. Quantum Electron. **42**, 160–170 (2006).
30. N. Bhat and J. Sipe, "Optical pulse propagation in nonlinear photonic crystals," Phys. Rev. E **64**, 056604 (2001).
31. M. Santagiustina, C. G. Someda, G. Vadalà, S. Combrié, and A. D. Rossi, "Theory of slow light enhanced four-wave mixing in photonic crystal waveguides," Opt. Express **18**, 21024–21029 (2010).
32. J. F. McMillan, M. Yu, D.-L. Kwong, and C. W. Wong, "Observation of spontaneous raman scattering in silicon slow-light photonic crystal waveguides," Appl. Phys. Lett. **93**, 251105 (2008).
33. M. Bahl, N.-C. Panoiu, and R. M. Osgood, "Nonlinear optical effects in a two-dimensional photonic crystal containing one-dimensional kerr defects," Phys. Rev. E **67**, 056604 (2003).
34. D. Michaelis, U. Peschel, C. Wächter, and A. Bräuer, "Reciprocity theorem and perturbation theory for photonic crystal waveguides," Phys. Rev. E **68**, 065601 (2003).
35. C. Monat, B. Corcoran, D. Pudo, M. Ebnali-Heidari, C. Grillet, M. D. Pelusi, D. J. Moss, B. J. Eggleton, T. P. White, L. O'Faolain, and T. F. Krauss, "Slow light enhanced nonlinear optics in silicon photonic crystal waveguides," IEEE J. Selec. Quantum Electron. **16**, 344–356 (2010).
36. A. W. Snyder and J. D. Love, *Optical Waveguide Theory* (Chapman and Hall, 1995).
37. J. A. Buck, *Fudamentals of Optical Fibers* (John Wiley & Sons, 2004).
38. P. Petropoulos, H. Ebendorff-Heidepriem, V. Finazzi, R.C. Moore, K. Frampton, D.J. Richardson and T.M. Monro, "Highly nonlinear and anomalously dispersive lead silicate glass holey fibers," Opt. Express **11**, 3568–3573 (2003).
39. E. C. Mägi, L. B. Fu, H. C. Nguyen, M. R. E. Lamont, D. I. Yeom, and B. J. Eggleton, "Enhanced Kerr nonlinearity in sub-wavelength diameter As_2Se_3 chalcogenide fiber tapers," Opt. Express **15**, 10324–10329 (2007).
40. T. M. Monro and H. Ebendorff-Heidepriem, "Progress in microstructured optical fibers," Ann. Rev. of Mater. Res. **36**, 467-495 (2006).
41. W. Q. Zhang, S. Afshar V. and T. M. Monro, "A genetic algorithm based approach to fiber design for high coherence and large bandwidth supercontinuum generation," Opt. Express **17**, 19311–19327 (2009).

#191963 - $15.00 USD Received 10 Jun 2013; revised 12 Jul 2013; accepted 14 Jul 2013; published 26 Jul 2013

1. Introduction

The nonlinear Schrödinger equation (NSE) describes pulse propagation in Kerr nonlinear dispersive media both for bulk and waveguides [1, 2]. In bulk materials, nonlinear optical Kerr effects are described through the modification of the refractive index, which in its simplest form is represented by $n = n_0 + n_2 I$, where n_2 is the nonlinear refractive index of the medium and $I = P/A$ is the light intensity (P and A are laser power and beam size, respectively). For weakly guiding waveguides, such as waveguides with low refractive index contrast or large core radius, a NSE can be developed for the amplitude of the propagating pulse, for which the nonlinear term, for a Kerr nonlinearity, is $\gamma |a(z,t)|^2 a(z,t)$, with nonlinear Kerr coefficient

$$\gamma = \frac{2\pi}{\lambda}\frac{n_2}{A_{\text{eff}}}, \qquad \text{where} \qquad A_{\text{eff}}^{(1)} = \frac{(\int_\infty |\mathbf{e}_t|^2 dA)^2}{\int_\infty |\mathbf{e}_t|^4 dA}. \tag{1}$$

Here, $a(z,t)$ is the amplitude of the specific mode, normalized such that $|a(z,t)|^2$ is the power in the mode, $\mathbf{e}_t$ is the transverse component of the electric field of the propagating modes, and $A_{\text{eff}}^{(1)}$ is its effective mode area. The integrals in Eq. (1) are taken over the entire cross section. In the weak guidance approximation the longitudinal (z)-component of a propagating mode vanishes hence the modes are purely transverse [2]. For both bulk materials and weakly guiding waveguides, the effective nonlinearity is proportional to the average intensity of light which is related to the mode power through the effective area [3, 4].

Over the last decade, a new class of optical waveguides with inhomogeneous or periodic structures, high refractive index contrast and subwavelength features including metallic layers, have attracted interest because of their large nonlinearity and possible applications for devices for all-optical data processing. Here, we refer to these waveguides as high index subwavelength waveguides (HIS-WGs). Examples of HIS-WGs include photonic crystal devices (waveguides with periodic structures) [5-8], silicon photonics [9-14], chalcogenide photonics [15-17], soft glass microstructured photonic devices [18-22], and hybrid glass-metal photonic devices [23, 24]. HIS-WGs operate in the strong guidance regime where Eqs. (1) no longer hold. In this regime, Eq. (1) not only underestimates the value of the Kerr effective nonlinear coefficient γ [20], but also fails to predict the structural dimensions required to obtain maximum γ, even for a simple glass-air step index geometry (see Fig. 1(a) for example). It has been shown experimentally, that Eq. (1) underestimates the value of γ by more than a factor of 2 for a bismuth-air step index in the strong guidance regime [20]. Hence a generalization of Eq. (1) is required in order to calculate the strength of the nonlinear effect, and to design a fiber or waveguide so as to optimize nonlinear phenomena. Ideally, the generalization of Eq. (1) would include, in addition to the effect of the effective area, the effect of the mode's longitudinal field components, its group velocity, as well as the nonuniform distribution of the nonlinearity of the constituent materials over the cross section.

Different definitions of the effective (Kerr) nonlinearity have been developed for longitudinally invariant HIS-WGs, [25, 26, 27, 3, 4, 28]. Some of these definitions have borrowed the idea that "nonlinearity is proportional to intensity," from studies in the weak guidance regime, to relate the effective nonlinearity to the effective mode area and thus several definitions have been proposed for effective mode area. On the other hand, the dependence of the effective nonlinear coefficient on group velocity has received little attention. To the best of our knowledge, Chen *et. al.* [29] were the only group which appear to have developed a coupled mode theory for nonlinear processes, including the Raman effect, in silicon wires and showed explicitly that the nonlinear coefficient depends on group velocity. However, in their work no definition is given for the effective area of a mode and the nonlinear coefficient is normalized to the physical area of the nonlinear material, hence making it difficult to physically interpret.

#191963 - $15.00 USD Received 10 Jun 2013; revised 12 Jul 2013; accepted 14 Jul 2013; published 26 Jul 2013

For structures that guide light by using periodically structured cladding materials, such as photonic crystal waveguides, the effect of group velocity and the enhancement of different types of nonlinear processes due to slow light has been studied extensively both theoretically [30, 8, 31] and experimentally [32, 33, 7]. Though the effective nonlinear coefficient is shown to be proportional to $1/v_g^2$, [30, 8, 31] different definitions for the effective mode area in these waveguides have been given [8, 35].

Here, we resolve the ambiguity in the definition of the effective area of optical modes in waveguides which are longitudinally invariant. We compare different definitions of the effective nonlinearity γ which include definitions for the effective area A_{eff}, and show how accurately they can describe nonlinear phenomena both in the weak and strong guidance regimes. We also show that an argument based only on the light intensity in the nonlinear region does not give a complete description of the effective nonlinearity of a waveguide, regardless of how A_{eff} is defined. Furthermore, based on the full vectorial NSE developed by Afshar *et. al.* [27], we develop a new and general form of the effective nonlinear coefficient and explicitly show that in the form developed here, γ depends on the contribution of three physical parameters; the distribution of nonlinearity of the waveguide's constituent materials over the waveguide cross section and its overlap with the field, the area of the propagating mode represented by the effective area A_{eff}, and the group velocity of the mode. While we acknowledge the freedom to factorize γ in different ways, we believe that factorization developed here provides the most appealing definition since it leads to a form of γ that combines group velocity, effective area, and nonlinear overlap integral in a physically meaningful way.

The outline of the paper is as follows. In Section 2, we introduce two different factorizations of the effective nonlinear coefficient, γ, which are based on the effective area and slow light. This is then followed by the results Section, 3, in which we compare the behavior of different definitions of effective areas and effective nonlinear coefficients of the HE_{11}, TE_{01} and TM_{01} modes of a step-index, glass-air fiber as a function of core radii. We compare the behavior of the group velocities of these modes as a function of core radius and explain how it relates to the maxima of the effective nonlinear coefficients of the HE_{11}, TE_{01} and TM_{01} modes. We also analyze the contributions to γ for step-index fibers with different values of the core-cladding refractive index contrast. Finally, we present the conclusion and a brief discussion of our results.

2. Theory

We consider a full vectorial description of nonlinear pulse propagation in a single mode optical waveguide as developed by Afshar *et. al* [27, Eq. (38)]

$$\frac{\partial}{\partial z}a(z,t) - i\sum_n \frac{(i\partial/\partial t)^n}{n!}\beta^{(n)}a(z,t) = i\gamma^V |a(z,t)|^2 a(z,t), \tag{2}$$

where $a(z,t)$ is the amplitude of the propagating pulse, $\beta^{(n)}$ are the $n-$th order dispersion coefficients, and γ^V is given by

$$\gamma^V = \frac{2\pi}{\lambda}\frac{\varepsilon_0}{\mu_0}\frac{\int_\infty n^2(x,y)n_2(x,y)[2|\mathbf{e}|^4 + |\mathbf{e}^2|^2]dA}{3\left|\int_\infty (\mathbf{e}\times\mathbf{h}^*)\cdot\hat{z}dA\right|^2}. \tag{3}$$

Here, $\mathbf{e}(x,y)$ and $\mathbf{h}(x,y)$ are the electric and magnetic field distribution of a particular propagating mode, n and n_2 are the linear and nonlinear refractive index distributions, respectively, and ε_0 and μ_0 are the permittivity and permeability of vacuum, respectively.

The coefficient γ^V in Eq. (3) was obtained through the development of nonlinear pulse propagation equation, Eq. (2), which is based on the full vectorial Maxwell equations [27]. Hence, this expression completely determines the effective Kerr nonlinearity of a pulse as it propagates

#191963 - $15.00 USD Received 10 Jun 2013; revised 12 Jul 2013; accepted 14 Jul 2013; published 26 Jul 2013

through a waveguide, as was confirmed experimentally for propagation through a nanowire [20]. We therefore take it to be the correct expression for the effective nonlinearity of an optical waveguide. Equation (3) has two important elements: the strength of electric field through $|\mathbf{e}|^4$ and $\left|\mathbf{e}^2\right|^2$, which originates from the nonlinear polarization vector, and the power flow $\int_\infty(\mathbf{e}\times\mathbf{h}^*)\cdot\hat{z}dA$, which originates from mode orthogonality.

One way to present γ^V, in analogy to Eq. (1), is to factor $(2\pi/\lambda)n_{2,core}$ in Eq. (3) and define the remainder as the effective area A_{eff}, *i.e.*,

$$\gamma^V=\frac{2\pi}{\lambda}\frac{n_{2,core}}{A_{\text{eff}}},\qquad\text{where}\qquad A_{\text{eff}}=\frac{\mu_0}{\varepsilon_0}\frac{3n_{2,core}\left|\int_\infty(\mathbf{e}\times\mathbf{h}^*)\cdot\hat{z}dA\right|^2}{\int_\infty n^2(x,y)n_2(x,y)[2\left|\mathbf{e}\right|^4+\left|\mathbf{e}^2\right|^2]dA}. \tag{4}$$

For glass-air step index fibers, assuming that the n_2 of the air is negligible, this reduces to [28]:

$$A_{\text{eff}}=\frac{\mu_0}{\varepsilon_0}\frac{3\left|\int_\infty(\mathbf{e}\times\mathbf{h}^*)\cdot\hat{z}dA\right|^2}{n_{core}^2\int_{\text{NL}}[2\left|\mathbf{e}\right|^4+\left|\mathbf{e}^2\right|^2]dA}. \tag{5}$$

The A_{eff} in Eq. (4) accurately describes the behavior of γ^V in both the strong and weak guidance regimes. However, it does not separate the linear and nonlinear effects; even in its simplest form (5) is difficult to interpret physically since it involves both the integral of the $z-$component of Poynting vector, representing the power flow, and the square of electric field intensity due to the nonlinear polarization. As a result, alternative factorizations are desirable.

Different ways to factorize γ^V can be conceived. In the following we discuss two factorizations based on *effective area* and *slow light* and show that while these factorizations are useful to obtain insight in the effective nonlinearity of a specific waveguide, these elements do not, by themselves, provide a complete description of the effective nonlinearity.

2.1. Factorization based on effective area

Following Afshar *et al.* [27], we define

$$A_{\text{eff}}^{(2)}=\left|\int_\infty(\mathbf{e}_\nu\times\mathbf{h}_\nu^*)\cdot\hat{z}dA\right|^2\Big/\int_\infty\left|(\mathbf{e}_\nu\times\mathbf{h}_\nu^*)\cdot\hat{z}\right|^2dA, \tag{6}$$

and use it to factorize γ in Eq. (3) as

$$\gamma^V=\frac{2\pi}{\lambda}\frac{\overline{n_2}}{A_{\text{eff}}^{(2)}},\qquad\text{where,}\qquad\overline{n_2}=\frac{\varepsilon_0}{\mu_0}\frac{\int_\infty n^2(x,y)n_2(x,y)[2\left|\mathbf{e}_\nu\right|^4+\left|\mathbf{e}_\nu^2\right|^2]dA}{3\int_\infty\left|(\mathbf{e}_\nu\times\mathbf{h}_\nu^*).\hat{z}\right|^2dA}, \tag{7}$$

where $\overline{n_2}$ can be viewed as an effective nonlinear refractive index, averaged over the waveguide's inhomogeneous cross section, weighted with respect to the electric field distribution. For this factorization, $A_{\text{eff}}^{(2)}$ is the propagating mode's effective area, which depends only on the geometry and the linear refractive index of the waveguide $n(x,y)$. It represents the area of longitudinal power flow, since $(\mathbf{e}\times\mathbf{h}^*)\cdot\hat{z}$ is the z-component of the Poynting vector. In general $\overline{n_2}\neq n_2$, even for a step index waveguide for which in the cladding typically $n_2=0$, indicating that $\gamma^V\neq(2\pi/\lambda)n_2/A_{\text{eff}}^{(2)}$, *i.e.*, γ^V, in contrast to γ in Eq. (1), cannot be fully described by $A_{\text{eff}}^{(2)}$.

2.2. Factorization based on slow light

The group velocity of a propagating mode of a waveguide made from a non-magnetic material (*i.e.*, $\mu=\mu_0$) can be related to its field distribution through [36, Eq. (31-30)]

$$v_g=-\frac{\frac{1}{2}\int_\infty(\mathbf{e}\times\mathbf{h}^*)\cdot zdA}{\frac{\lambda^2}{4}\int_\infty\{\varepsilon_0|\mathbf{e}|^2\frac{d}{d\lambda}\frac{n^2}{\lambda}-\frac{\mu_0}{\lambda^2}|\mathbf{h}|^2\}dA}, \tag{8}$$

#191963 - $15.00 USD Received 10 Jun 2013; revised 12 Jul 2013; accepted 14 Jul 2013; published 26 Jul 2013

which reduces to

$$v_g = \frac{2\int_\infty \mathbf{e}\times\mathbf{h}^*\cdot z dA}{\varepsilon_0\int_\infty [2n^2-(\lambda dn^2/d\lambda)]|\mathbf{e}|^2 dA},$$

since the stored electric and magnetic energies are equal [36, Eq. (31-24)]. By ignoring $\lambda dn^2/d\lambda$, v_g can be written as

$$v_g = \frac{\int_\infty \mathbf{e}\times\mathbf{h}^*\cdot z dA}{\varepsilon_0\int_\infty n^2|\mathbf{e}|^2 dA}. \tag{9}$$

For bismuth glass, for example, $\lambda(dn^2/d\lambda) < 0.06n^2$ over the entire wavelength range $1-2\ \mu$m. The approach below assumes the inequality $\lambda(dn^2/d\lambda) \ll 2n^2$ to hold; in cases it does not then the factor n^2 can be replaced by $n^2-(\lambda/2)(dn^2/d\lambda)$ in subsequent equations.

We use Eq. (9) to factorize γ^V in Eq. (3) as

$$\gamma^V = \frac{2\pi}{\lambda}\left(\frac{c}{n_{core}v_g}\right)^2 \frac{n_2^{avg}}{A_{\text{eff}}^{(3)}} \tag{10}$$

in which

$$n_2^{avg} = \frac{n_{core}^2\int_\infty n^2 n_2[2|\mathbf{e}|^4+|\mathbf{e}^2|^2]dA}{3\int_\infty n^4|\mathbf{e}|^4 dA}, \quad \text{and} \quad A_{\text{eff}}^{(3)} = \frac{(\int_\infty n^2|\mathbf{e}|^2 dA)^2}{\int_\infty n^4|\mathbf{e}|^4 dA}. \tag{11}$$

To the best of our knowledge this is the first time a rigorous expression for the effective nonlinearity of a waveguide is related to the modal group velocity v_g as in Eq. (10). In addition, Eqs (10) and (11), provide alternative definitions $A_{\text{eff}}^{(3)}$, and n_2^{avg}. The new definition of mode area $A_{\text{eff}}^{(3)}$ reduces to the scalar expression $A_{\text{eff}}^{(1)}$ from Eq. (1) in the appropriate limit. Equation (10) explicitly indicates that the nonlinearity of a waveguide is determined by three factors; (1) the nonlinearity of the waveguide material through the nonlinear refractive index; (2) the area of the electric field intensity distribution, *i.e.*, how tightly the electric field is confined to the nonlinear material; and (3) the square of group velocity of the mode.

Having established an exact factorization of γ^V we now consider two approximations. In the first of these we use the observation of Lægsgaard [28] that $|\mathbf{e}|^4 = e_t^4+e_z^4+2e_t^2e_z^2 \approx |\mathbf{e}^2|^2 = e_t^4+e_z^4-2e_t^2e_z^2$ (see also discussion in Section 3), for which we have used the fact that the propagating modes of a waveguide can be constructed such that $\mathbf{e_t}$ (transverse component of the electric field) and e_z (longitudinal component of the electric field), respectively, are purely real and imaginary [36, Eq. (11-8)]. Using this result in Eq. (11) we can write n_2^{avg} as

$$n_2^{avg} \approx \frac{n_{core}^2\int_\infty n^2 n_2|\mathbf{e}|^4 dA}{\int_\infty n^4|\mathbf{e}|^4 dA}. \tag{12}$$

This expression is physically more meaningful than $\bar{n}_2$ (Eq. (7)) since it represents an averaged value of n_2, weighted by the fourth power of the electric field strength $|e|^4$.

We can simplify this result yet more for waveguides with a single nonlinear constituent, for example a step-index fiber or waveguide in air. For such fibers the integral in the numerator of Eq. (12) reduces to the product of the nonlinear coefficient and an integral which involves only linear properties, *viz.*

$$n_2^{avg} \approx n_2\frac{n_{core}^4\int_{NL}|\mathbf{e}|^4 dA}{\int_\infty n^4|\mathbf{e}|^4 dA}, \tag{13}$$

where the second factor characterizes the degree to which the modal field overlaps the nonlinear region. As mentioned, it depends on $|e|^4$ since this is a nonlinear overlap. The advantage of Eq. (13) is that it separates this overlap, which cannot exceed unity, from the actual value of the nonlinear coefficient. We illustrate the use of this factorization in Section 3.

#191963 - $15.00 USD Received 10 Jun 2013; revised 12 Jul 2013; accepted 14 Jul 2013; published 26 Jul 2013

3. Results

To understand the contribution of the effective area on the effective nonlinear coefficient γ in both the strong and weak guidance regimes, we consider $A_{\rm eff}^{(2)}$ and $A_{\rm eff}^{(3)}$ and other definitions of $A_{\rm eff}$ reported in the literature. We use these in the first of Eq. (1) and compare them with γ from Eq. (7) for step-index nanowires with high index contrast and varying core radii. We consider

$$A_{\rm eff}^{(4)} = a_{\rm NL} \int_{\infty} \mathbf{S}_z dA / \int_{\rm NL} \mathbf{S}_z dA, \tag{14}$$

$$A_{\rm eff}^{(5)} = 2\pi \int_{\infty} r^2 \mathbf{S}_z dA / \int_{\infty} \mathbf{S}_z dA, \tag{15}$$

$$A_{\rm eff}^{(6)} = \left(\int_{\infty} |\mathbf{e}_t|^2 dA \right)^2 / \int_{\rm NL} |\mathbf{e}_t|^4 dA, \tag{16}$$

reported respectively in [4, 25, 26] where $a_{\rm NL} = \pi \omega_{\rm NL}^2$ is the physical area of the nonlinear region (with the radius of $\omega_{\rm NL}$) and NL indicates integration over the nonlinear region.

The left-hand side of Fig. 1 shows $A_{\rm eff}^{(i)}$ for $i = 1, 2, \ldots 6$ versus core radius at $\lambda = 1550$ nm for the HE_{11} (a), TE_{01} (c) and TM_{01} (e) modes of a step-index bismuth-air fiber. For bismuth we have taken $n = 2.018$, $n_2 = 6.0 \times 10^{-19}$ m^2/W [20]. For all modes and for all definitions of the effective area the curves exhibit similar behavior: for large core radii (the weak guidance regime) the degree of confinement is low and the effective area is large; for very small core radii, the refractive index contrast is insufficient to confine the mode, and the field extends substantially into the cladding. Between these extremes, in the strong guidance regime, the effective area attains a minimum value where the index contrast leads to strong confinement. However, while sharing the same general characteristics, the different definitions lead to different minimum values at different core radii.

The right-hand side of Fig. 1 shows the associated $\gamma^{(i)}$ calculated from the first of Eqs (1) and also the full vectorial γ^V from Eq. (7) (dashed red curve). None of the $\gamma^{(i)}$ match γ^V in the strong guidance regime–thus, none of the effective areas $A_{\rm eff}^{(i)}$ ($i = 1, \ldots, 6$) in themselves accurately describe the behavior of γ.

All definitions of $A_{\rm eff}^{(i)}$, except $A_{\rm eff}^{(4)}$, do have the same asymptotic behavior for large core radii, *i.e.*, approaching weak guidance regime. In this regime, therefore, any of $A_{\rm eff}^{(i)}$ for $i = 1-3, 5, 6$ can be used to calculate the effective mode area and the effective nonlinearity. The reason why $A_{\rm eff}^{(4)}$, defined in Eq. (14) behaves differently is that it was constructed so as to approach the physical area of nonlinear region $\pi \omega_{\rm NL}^2$, in the weak guidance limit. However, it was pointed out previously (see for example Chapter 3 in [37]) that in this limit the transverse optical power distribution can be approximated by a Gaussian function with a width which is less than the geometrical fiber core radius. This is illustrated in Figs. 1 (a), (c), and (e), in which $A_{\rm eff}^{(i)} < A_{\rm eff}^{(4)}$ ($i = 1-3, 5, 6$) for large core radii up to 1.0 μm.

We now briefly discuss the features of some of the other definitions of $A_{\rm eff}$. For the TE_{01} mode $A_{\rm eff}^{(1)} = A_{\rm eff}^{(2)}$ and $\gamma^{(1)} = \gamma^{(2)}$ since electric field has no $z-$component. Nonetheless, $\gamma^{(1,2)} \neq \gamma^V$ since $\overline{n_2} \neq n_2$. This indicates the importance of $\overline{n_2}$ for the effective nonlinearity. Note also that $A_{\rm eff}^{(1)}$ and $\gamma^{(1)}$ which have been used for many years and are discussed extensively in the textbook by Agrawal [2] were derived for the weak guidance regime only and cannot be expected to have wider validity. Even though definition (6) exhibits the correct behavior in the weak-guidance limit, it deviates strongly from γ^V at smaller core radii. This is because $A_{\rm eff}^{(6)}$ only includes the transverse electric field component, which is not sufficient in the strong guidance regime. Note also that $A_{\rm eff}^{(6)} > A_{\rm eff}^{(1)}$ since its denominator integral is taken only over the fiber core, and thus $\gamma^{(6)} < \gamma^{(1)}$. As to definitions 2, 3, and 5, in the weak guidance regime, $|e|^2 \propto S_z$, and

#191963 - $15.00 USD Received 10 Jun 2013; revised 12 Jul 2013; accepted 14 Jul 2013; published 26 Jul 2013

assuming a Gaussian function of radial distance with a radius of ω for both S_z and $|e|^2$, *i.e.*, $S_z \propto \exp(-r^2/\omega^2)$ [4] for the HE_{11}, leads to $A_{\text{eff}}^{(2)} = A_{\text{eff}}^{(3)} = A_{\text{eff}}^{(5)} = 2\pi\omega^2$. This is evident in Figs. 1 (a), in which $A_{\text{eff}}^{(2)} \approx A_{\text{eff}}^{(3)} \approx A_{\text{eff}}^{(5)}$ for large core radii up to 1.0 μm. Similar behavior is observed for the TE_{01} and TM_{01} modes in Figs. 1 (c) and (e). In the strong guidance regime, $A_{\text{eff}}^{(5)}$ deviates from $A_{\text{eff}}^{(2)} = A_{\text{eff}}^{(3)}$ and leads to $\gamma^{(5)}$ values that are smaller than those of $\gamma^{(2)}$, $\gamma^{(3)}$, and γ^V, as shown in Figs. 1(b), (d), and (f).

Definitions (2) and (3) for the effective area were obtained by different factorizations of γ^V in Eq. (3). Definition (2) is based on the Poynting vector and estimates the area of energy flow. In contrast, $A_{\text{eff}}^{(3)}$ is defined based on the electric field intensity and represents its area. These two definitions are related implicitly through the group velocity v_g (Eq. (9)). While both definitions approach each other for large radii for all three modes, they are significantly different in the strong-guidance limit for TE_{01} and TM_{01} modes. Both $A_{\text{eff}}^{(2)}$ and $A_{\text{eff}}^{(3)}$ in conjunction with other parameters in Eqs. (3) and (10), respectively, lead to γ^V and hence both can be equivalently considered as the effective area of a mode. However, as we show next, the factorization in definition (3) leads to the most physically-meaningful factorization since it leads to the explicit dependence of γ^V on group velocity, effective area and nonlinear overlap integral.

Figure 2 shows how the parameters, n_2^{avg}, v_g, $A_{\text{eff}}^{(3)}$ and γ^V depend on the core radius for the three lowest modes of a bismuth step-index fiber. The plot of n_2^{avg} in Fig. 2(a) shows that as the core radius increases, and the propagating mode spreads within the nonlinear core region, the n_2^{avg} asymptotically approaches a maximum value, which is below the nonlinear refractive index of the core, *i.e.*, n_2. In contrast, due to slow-light effects, for all three modes $\overline{n_2}$ has maximum above the n_2 of the core material. Comparing $\overline{n_2}$ and n_2^{avg}, the latter is physically more meaningful; it represents an averaged value of n_2, *i.e.*, how much of nonlinear material is accessed by the electric field.

Figure 2 (b) shows the group velocities v_g of the three modes HE_{11}, TE_{01}, and TM_{01} versus core radius. At small core radii, where the modal fields spread outside the core region, the group velocities of the modes equal the speed of light in air c, and approach that of the glass $c/n = c/2.018$ as the core radius increases and the modes mostly reside inside the glass core. However, the group velocities of all three modes reach a minimum for some core radius, indicating that $(\partial/\partial R)v_g = 0$ (R is the core radius) here. This can be explained by noting that instead of examining v_g versus core radius (at constant wavelength) one can equivalently study the behavior of v_g versus wavelength (at constant core radius), which is correct if we ignore material dispersion. Hence, the existence of minima in group velocities is equivalent of having a zero group velocity dispersion for the three modes, *i.e.*, $D = 0$, where $D = d\beta_1/d\lambda = (-2\pi c/\lambda^2)\beta_2$ is the dispersion parameter and β_2 is the second order dispersion [2].

Figures 2 (b) and (d) show that, consistent with Eq. (10), the minima of the group velocities of the three modes approximately coincide with the maxima of their γ^V values, indicating that the enhancement of Kerr effect is due to slow light effects. Note though that we are considering a simple step index air-glass fiber without any structural optimization. It is possible to design microstructured optical fibers and photonic crystal waveguides so as to reduce the minimum group velocities at a certain wavelength so the effect would become more pronounced [35]. Of course, to achieve a maximum γ^V both A_{eff} and v_g, would need to be optimized simultaneously.

By comparing γ^V, n_2^{avg}, $A_{\text{eff}}^{(3)}$, and v_g of the three modes as a function of core radius (see Figs. 2 (a)-(d)), it is observed that the minima of v_g and A_{eff} do not coincide for all the modes, so the maxima of γ lie between the minima of v_g and A_{eff}. Furthermore, although the minima of v_g are roughly the same for the three modes, there is a significant difference of about a factor two between their maxima, indicating that for a step-index fiber the effective area is the main factor in determining γ^V. This is consistent with Fig. 2(c), where a significant difference is

#191963 - $15.00 USD Received 10 Jun 2013; revised 12 Jul 2013; accepted 14 Jul 2013; published 26 Jul 2013

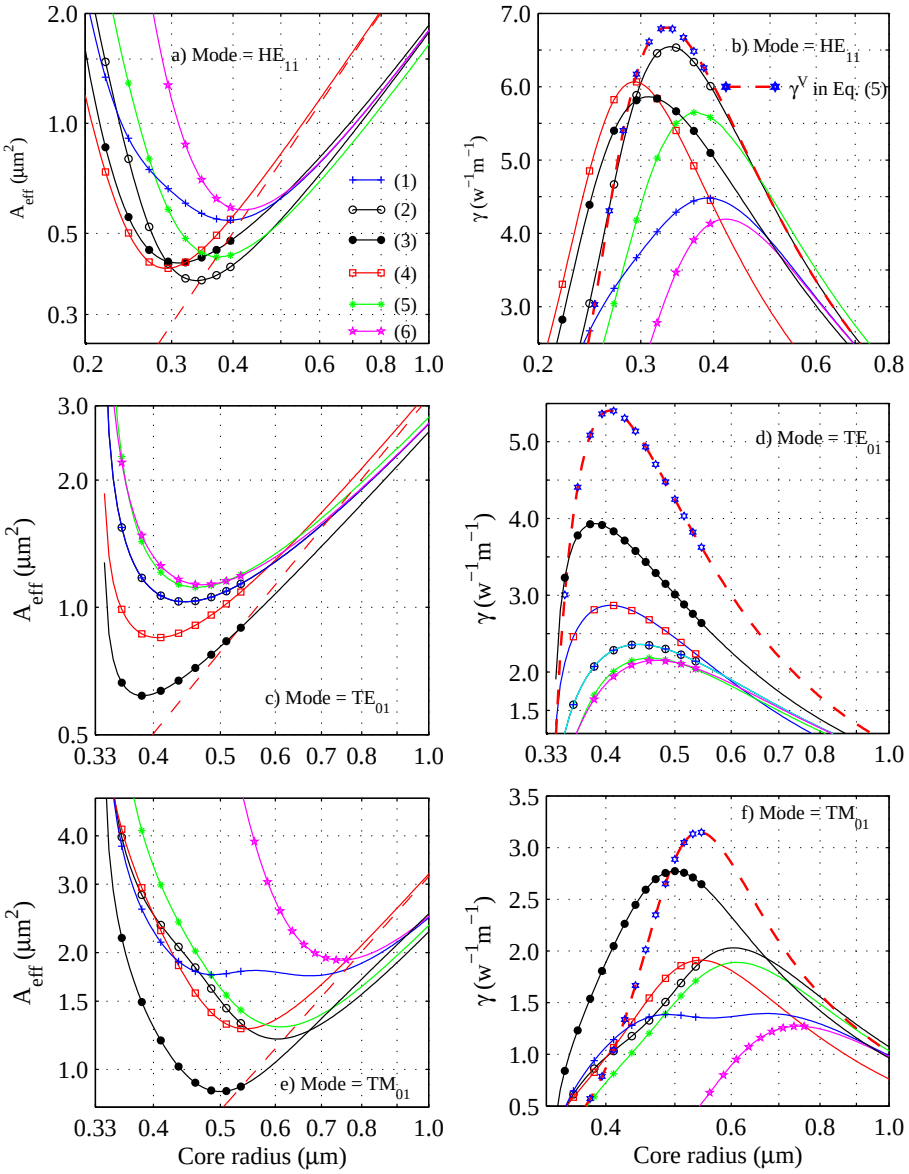

Fig. 1. (a), (c) and (e): Effective area $A_{\text{eff}}^{(i)}$, $i = 1, 2, \ldots, 6$; and (b), (d), (f): $\gamma^{(i)}$ as well as γ^V, versus core radius for a bismuth-air step index fiber and for (a) and (b): the HE_{11} mode; (c) and (d) TE_{01}; and (e) and (f) TM_{01}. The $A_{\text{eff}}^{(i)}$ are calculated from Eqs. (1), (6), (11), (14)-(16). Inset in (a) shows the color code for each of $i = 1, 2, ..., 6$. The dashed lines in (a), (c), and (e) show the geometrical area of the fiber core.

observed between the minima of the effective areas of the modes. In summary, while none of A_{eff}, v_g, and n_2^{avg} alone, regardless of how they have been defined, can give a complete picture of γ^V of a waveguide, we believe that the definition of $A_{\text{eff}}^{(3)}$ in Eq. (11) is the most appropriate way to define the effective area of a mode. This definition, in conjunction with v_g (Eq. (9)) and n_2^{avg} (Eq. (11)), provides a physically meaningful factorization of the effective nonlinear coefficient

#191963 - $15.00 USD Received 10 Jun 2013; revised 12 Jul 2013; accepted 14 Jul 2013; published 26 Jul 2013

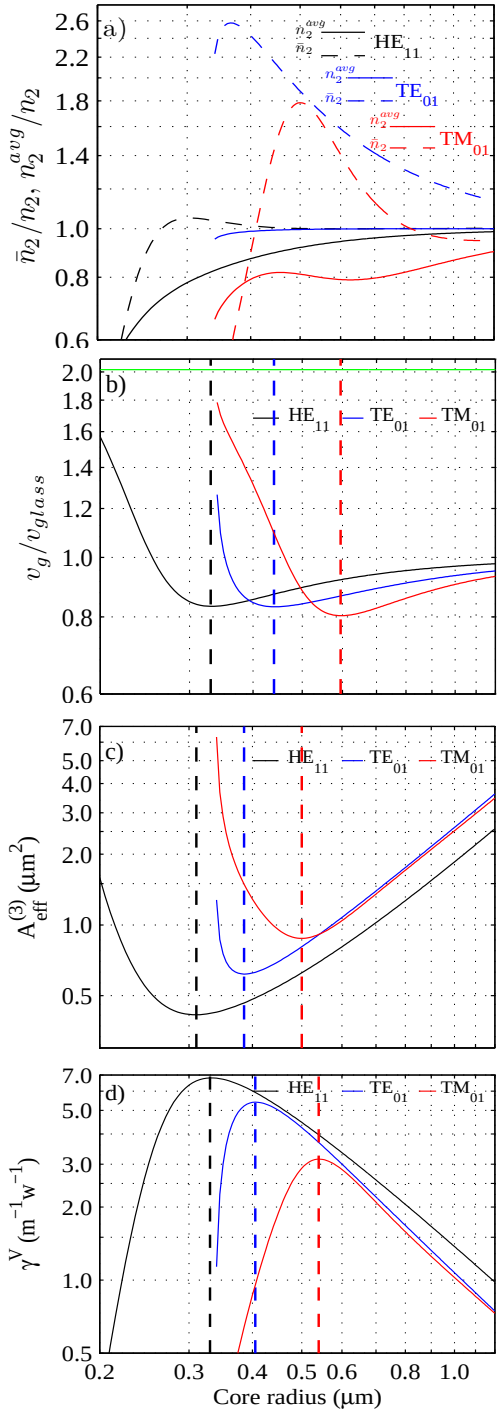

Fig. 2. (a)-(d): $\bar{n}_2$ and n_2^{avg} (normalized to n_2 of bismuth), v_g (normalized to the speed of light in the glass, c/n), $A_{\text{eff}}^{(3)}$, and γ^V, respectively, for HE_{11} (black), TE_{01} (blue), and TM_{01} (red) modes. Dashed curves in (a) show the behavior of $\bar{n}_2$, as defined in Eq. (7). Vertical dashed lines in figures (b)-(d) show the positions of minima, for v_g and A_{eff}, or maxima for γ^V. The solid horizontal green line in (b) represents the speed of light in air.

#191963 - $15.00 USD Received 10 Jun 2013; revised 12 Jul 2013; accepted 14 Jul 2013; published 26 Jul 2013

of a waveguide γ^V, showing that γ^V depends on the nonlinear refractive index distribution of the waveguides and its overlap with the electric field, the mode area, and the mode's group velocity.

The factorization (10) allows us to identify whether or not parameters $A_{\text{eff}}^{(3)}$, v_g and n_2^{avg} can be optimized simultaneously. Though Eq. (3) can be evaluated numerically it may be difficult to predict or understand its behavior without factorizing it into physically appealing constituents. For example, it is difficult to see how γ^V depends on the index contrast between the core and cladding materials of a glass-air step index waveguide.

To investigate this, we consider the minima of v_g and $A_{\text{eff}}^{(3)}$ of the HE_{11} mode of glass-air step index fibers versus core radius (see Figs. 2(b) and (c)). We then indicate these minima and their corresponding core radii as a function of the core refractive index in Figs. 3(a), (b), and (f), respectively. Also indicated are the the refractive indices of commonly used optical materials; silica ($n = 1.444$, $n_2 = 2.6 \times 10^{-20}$ m^2/W [2]), the lead glass SF57 ($n = 1.8$, $n_2 = 4.1 \times 10^{-19}$ m^2/W [38]), bismuth ($n = 2.018$, $n_2 = 6.0 \times 10^{-19}$ m^2/W [20]), and chalcogenide ($n = 2.8$, $n_2 = 1.1 \times 10^{-17}$ m^2/W [39]). The minimum values of both $A_{\text{eff}}^{(3)}$ and v_g reduce as the index contrast between the core and cladding increases, with the minimum of v_g reducing faster than the speed of light in the glass, $v_{glass} = c/n_{core}$.

In Fig. 3(c) we show n_2^{avg}/n_2 based on Eqs. (11) (solid curves) and the approximate Eq. (12) (dashed curves), as a function of core radius and for different core refractive indices. For a step index fiber this dependence is completely determined by the linear waveguide properties (see Eq. (13)), and asymptotically approaches unity as the core radius increases and the field is increasingly confined to the core. However, whereas n_2^{avg} increases monotonically as a function of core radius, the exact Eq. (11) exhibits non-monotonic behavior for high refractive indices ($n \gtrsim 2.4$), as indicated by the solid curves in Fig. 3(c). The difference is due to the approximation $|\mathbf{e}|^4 \approx |\mathbf{e}^2|^2$, which was used to obtain Eq. (12). This approximation is valid for large core radius and low index contrast waveguides, where the longitudinal component of the electric field e_z is much smaller than the transverse component e_t, but can results in as much as 25% difference in the exact and approximated values of n_2^{avg}, Eqs. (11) and (12), in the strong guidance regime (small core radius and large index contrast). At fixed core radius, n_2^{avg}/n_2 increases with increasing core refractive index.

Figure 3(d) shows the maximum of γ^V/n_2 versus core refractive index. This quantity is entirely determined by the linear fiber properties and it represents the overall effects of the effective mode area, $1/A_{\text{eff}}^{(3)}$, group velocity, $[c/(n_{core}v_g)]^2$, and the nonlinear overlap overlap n_2^{avg}/n_2 (see Eq. (10)). Once multiplied by the n_2 of the core material, this quantity represents the maximum achievable γ^V in step-index fibers versus core refractive index (see Fig. 3(e)). The values of n_2 for the core materials were obtained from Miller's rule [40], which gives an approximate relation between the linear and nonlinear properties of a wide class of media, based on which the solid curve has been obtained. The individual results indicated in red are based on the actual nonlinear properties of the four materials given above. Having found the maximum of γ^V, Fig. 3(f) indicates the core radii corresponding to minimum $A_{\text{eff}}^{(3)}$, minimum v_g, and maximum γ^v. The core radii corresponding to the maximum of γ^V is closer to that of the minimum of v_g, since it enters quadratically in the definition of γ^V (see Eq. (10)).

An implication of this analysis pertains to possible strategies for optimizing γ^V. Traditional approaches are based on minimizing the effective area and maximizing the nonlinear coefficient n_2. Equation (13) shows that the group velocity and overlap between the field and the nonlinear medium should also be optimized. The latter is perhaps not surprising but has limited scope since the overlap cannot exceed unity. The only remaining factor is the group velocity. Figure 3(b) shows that even though the group velocity decreases faster than c/n_{core}, this additional effect is modest. A possibly profitable route to increasing γ^V is therefore to devise waveguide

#191963 - $15.00 USD Received 10 Jun 2013; revised 12 Jul 2013; accepted 14 Jul 2013; published 26 Jul 2013

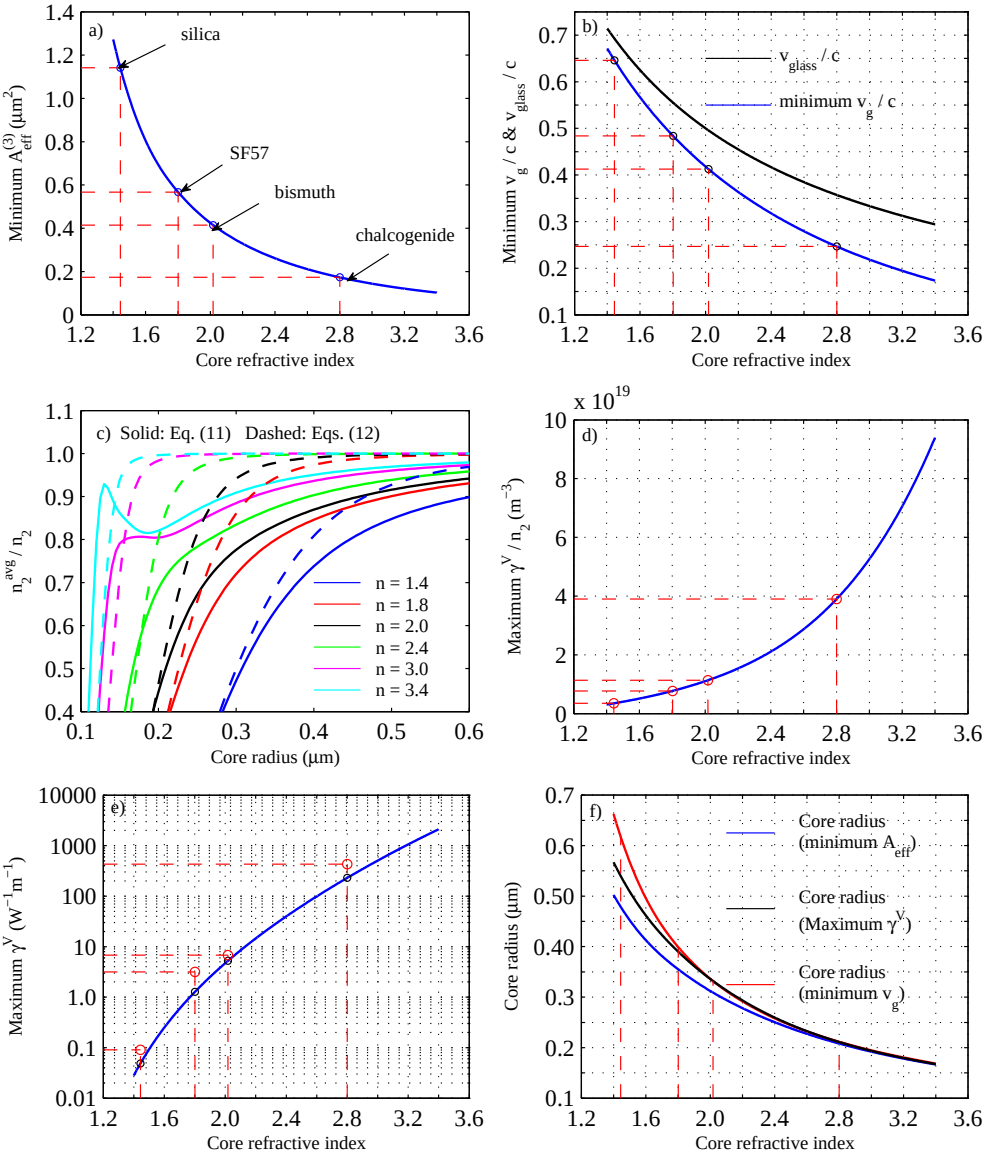

Fig. 3. Nonlinear properties of circular step-index fibers versus core refractive index, optimized with respect to core radius. Vertical dashed lines correspond to silica, SF57, bismuth, and chalcogenide. (a) Minimum of $A_{\text{eff}}^{(3)}$; (b) minimum v_g; (c) n_2^{avg}/n_2 versus core radius. Solid and dashed curves were evaluated based on Eqs. (11) and (12), respectively; (d) maximum of γ^V/n_2; (e) maximum of γ^V. The solid curve follows from Miller's rule, whereas the four red data points are for the specific n_2 values for the four materials. (f) Core radii corresponding to the minimum of $A_{\text{eff}}^{(3)}$ (blue), v_g (red), and maximum of γ^V (black), as a function of the refractive index.

#191963 - $15.00 USD Received 10 Jun 2013; revised 12 Jul 2013; accepted 14 Jul 2013; published 26 Jul 2013

designs with low group-velocity, while maintaining, of course, the small effective area and substantial nonlinear overlap. While the use of slow light is well-established in photonic crystal, we are not aware of systematic studies in the longitudinally invariant systems considered here. A more immediate implication of our work follows from Figs 3(e) and (f), which show, respectively, the very strong effect of increasing the core refractive index, and the required core radius to fully exploit this increased effective nonlinearity–the second of these can be used directly to design highly nonlinear step-index fibers.

4. Discussion and conclusion

Different definitions of the effective nonlinearity of an optical waveguide have been reported, which are based on arguments relating to the "intensity in the nonlinear region". As a result, different effective nonlinear coefficients γ have been considered with different definitions for A_{eff}. We compare different definitions of A_{eff} and the resulting γ from Eq. (1), with γ^V. The expression for γ^V was developed based on a full vectorial nonlinear analysis and was confirmed experimentally to accurately describe the effective nonlinearity of optical waveguides both in the strong and weak guidance regimes. We show that none of the reported definitions for A_{eff} accurately describe the full behavior of γ^V in the strong guidance regime. In the weak guidance regime, most definitions of A_{eff} approach each other as Eq. (1) then provides a better approximation of the effective nonlinearity of a waveguide.

We have also developed a new factorization Eq. (10) of the full effective nonlinear coefficient γ^V, which depends on three key parameters: the average nonlinearity of the material; the effective mode area; and the modal group velocity. While, we acknowledge that γ^V can be factorized in different ways, which is evident by other publications reporting different factorization [29, 27, 28], the factorization developed here is physically appealing as it explicitly includes the group velocity. In this factorization, A_{eff} is the area of the intensity of the electric field and n_2^{avg} is the average of n_2 of the constituent materials with respect to electric field intensity distribution. Hence, we propose to define A_{eff} as in Eq. (11).

Based on Eq. (10) the effective Kerr nonlinear coefficient of a waveguide depends on three parameters: n_2^{avg}, v_g, and A_{eff}. None of these parameters by themselves completely describe γ^V, especially since they all depend on the mode distribution and hence are implicitly related to each other. However, for particular waveguides, it could be possible that one or two of these parameters dominate in enhancing γ^V. The new factorization introduced here allows us to analyze the enhancement of γ^V. While it might be tempting to think that the effective nonlinearity is determined by the minimum effective mode area that can be achieved, we can now address as to whether it is possible to enhance the effective nonlinearity beyond the limit set by the effective area, by considering additionally the effects of n_2^{avg} and the group velocity v_g. The parameters v_g, and A_{eff} are completely determined by the linear refractive index distribution of the waveguide. However, whereas the parameter n_2^{avg} is in general determined by the nonlinear refractive index and electric field distribution, for the common case in which only one of the constituent materials is nonlinear, or in which the nonlinear effects are dominated by one of the constituents, the ratio n_2^{avg}/n_2 is also fully determined by the linear properties. Thus it would be possible to use methods such as genetic algorithm methods [41] to optimize waveguides structures for enhanced nonlinearity by minimizing both v_g, and A_{eff}, and maximizing n_2^{avg} simultaneously.

The method introduced in this study could be applied to other linear and nonlinear processes in optical waveguides. The origin of appearing v_g in γ^V can be understood by inspecting Eq. (3), in which electric fields are normalized to $\sqrt{\int_\infty (\mathbf{e}^{(i)} \times \mathbf{h}^{(i)}).zdA}$. However, considering Eq. (9), we may alternatively state that the electric fields are normalized to $\sqrt{v_g}$. All linear and nonlinear

#191963 - $15.00 USD Received 10 Jun 2013; revised 12 Jul 2013; accepted 14 Jul 2013; published 26 Jul 2013

light-matter interaction terms can be described through $\mathbf{e}\cdot\boldsymbol{\chi}^{(n)}\vdots\,\mathbf{e}^{(1)}\mathbf{e}^{(2)}\cdots\mathbf{e}^{(n)}$, (see Eqs. (10)-(17) in [27]), in which $\boldsymbol{\chi}^{(n)}$ is a susceptibility tensor rank $n+1$, and signs $\cdot$ and $\vdots$ show scalar dot and tensorial products, respectively. As a result, one can predict that linear processes, such as absorption, $\boldsymbol{\chi}^{(3)}$ nonlinear processes such as Kerr nonlinearity, and higher order nonlinear processes should scale with $1/v_g$, $1/v_g^2$, and higher powers of $1/\sqrt{v_g}$, respectively.

While the focus of this study was on longitudinally invariant waveguides, some similarities can be drawn between these waveguides and photonic crystal waveguides. The full vectorial NSE developed for longitudinally invariant waveguides, Eq. (2), is based on a reciprocity theorem and a perturbation theory, [27], in which the electric and magnetic fields of a perturbed waveguide (a waveguide that includes nonlinear and dispersion effects) are expanded based on the orthonormal propagating modes of an unperturbed waveguide. Recently, a similar NSE has been developed for photonic crystal waveguides based on a similar method as in [27], but using rather different orthonormal propagating modes, *i.e.*, Bloch modes of the photonic crystal waveguides [34, 8, 31]. This similarity indicates that the results obtained here may be extended to photonic crystal waveguides, however, the proof of this is beyond the scope of this study.

Acknowledgments

The authors would like to acknowledge ARC funding support (DP110104247). Tanya M. Monro acknowledges the support of an ARC Federation Fellowship (FF0883189)

#191963 - $15.00 USD Received 10 Jun 2013; revised 12 Jul 2013; accepted 14 Jul 2013; published 26 Jul 2013